Proc. Natl. Acad. Sci. USA
Vol. 92, pp. 6878–6882, July 1995
Biochemistry

Submillisecond folding of monomeric λ repressor

(dynamic NMR)

GUEWHA S. HUANG AND TERRENCE G. OAS

Department of Biochemistry, Duke University Medical Center, Durham, NC 27710

Communicated by Gordon G. Hammes, Duke University Medical Center, Durham, NC, April 20, 1995

ABSTRACT **The folding kinetics of a truncated form of the N-terminal domain of phage λ repressor [λ_{6-85}] has been investigated by using the technique of dynamic NMR. λ_{6-85} has been shown previously to fold in a purely two-state fashion. This allows the determination of folding and unfolding rates from simulation of the exchange-broadened aromatic resonances of Tyr-22. The folding kinetics were determined over a range of 1.35 to 3.14 M urea. The urea dependence of both folding and unfolding rate constants is exponential, suggesting that the rate-determining step is invariant at the urea concentrations studied. The folding and unfolding rates extrapolated to 0 M urea at 37°C are 3600 ± 400 s^{-1} and 27 ± 6 s^{-1}, respectively. The observed λ_{6-85} folding rate constant exceeds that of other fast-folding globular proteins by a factor of 14–54. The urea dependence of the folding and unfolding rate constants suggests that the transition state of the rate-determining step is considerably more exposed to solvent than previously studied protein-folding transition states. The surprising rapidity of λ_{6-85} folding and unfolding may be the consequence of its all-helical secondary structure. These kinetic results clearly demonstrate that all of the fundamental events of protein folding can occur on the submillisecond time scale.**

The elucidation of the mechanism by which proteins fold remains one of the most challenging problems of modern biology. The earliest events in protein folding are particularly difficult to study by current methods and can be important determininants of the overall reaction (1, 2). Time-resolved kinetic studies have established that many of these important early events occur in <1 ms and are complete within the dead time of the stopped-flow technique. This rapid folding phase has been detected by circular dichroism (CD), fluorescence, and NMR stopped-flow studies in many proteins and reflects the potential for proteins to fold on the submillisecond time scale (3–9). Ultrasonic attenuation and dielectric relaxation measurements indicate that isolated α-helices fold with relaxation times of 10^{-7} to 10^{-8} s, four to five orders of magnitude faster than rate constants observable by stopped-flow methods (10–12). This vast time-scale difference represents a major gap in our understanding of the fundamental early events in folding.

In principle, dynamic NMR methods can fill this time-scale gap. Exchange processes that interconvert chemically or conformationally distinct species on the 10-ms to 10-μs time scale can have profound effects on the shape and position of NMR peaks (13). Much faster processes, including motions of the fully native form, can be studied by relaxation time measurements (14–17). To date, dynamic NMR has not been used to measure overall protein folding rates, although it has been used to detect a folding intermediate of rat intestinal fatty acid-binding protein (18). Dynamic NMR-based protein folding studies are rare because the overall folding rates of most proteins are not fast enough to broaden NMR resonances (19–22).

However, there is a growing number of proteins observed to fold on the microsecond time scale (3, 23–25), and it is likely that their folding processes are similar to early folding events in proteins that fold more slowly. An example of a fast-folding protein is the N-terminal domain (residues 1–102) of bacteriophage λ repressor *c*I, which has been used extensively as a model system (26). The crystal structure of residues 1–92 bound to DNA has been determined to 1.8-Å resolution (27). A truncated form containing residues 6–85 (λ_{6-85}) is monomeric and has a solution structure and stability that are essentially identical to those of the longer versions (28). A structural model for λ_{6-85} based on NMR data and the cocrystal structure of the λ_{1-92}–DNA complex, is shown in Fig. 1. NMR and CD studies have shown that the protein folds in a two-state fashion when denatured thermally or in urea, thus making it possible to interpret the NMR line shapes in terms of two interconverting species (28). In this report we describe the application of the line-shape method to measure the overall folding rate of λ_{6-85}.

MATERIALS AND METHODS

λ_{6-85} protein was expressed and purified as described (28). NMR samples consisted of 500 μM protein dissolved in NMR buffer [≈99% ^2H_2O/10 mM $C^2H_3COO^2H$/100 mM NaCl/3-(trimethylsilyl)propionic acid (17 μg/ml)/1 mM NaN_3, pH 5.6] with various concentrations of urea as determined by refractometry (30). Each sample was equilibrated at 37°C for at least 20 min prior to acquisition of the NMR spectrum.

Proton NMR spectra (1024 transients) were acquired at each urea concentration on a Varian Unity spectrometer at 500 MHz, by using presaturation for 1.5 s to suppress residual water. This recycle delay is sufficiently long to allow complete recovery of all protein signals. NMR data were processed by using FELIX 2.05 (Biosym Technologies, San Diego) and referenced to 3-(trimethylsilyl)propionic acid for each urea concentration. Line-shape simulations were computed by using a FELIX macro/accessory program (ZELIG) kindly provided by Michael Strain (University of Oregon).

RESULTS AND DISCUSSION

As demonstrated (28), the folding reaction of λ_{6-85} can be described by using the simple model:

$$N \underset{k_f}{\overset{k_u}{\rightleftharpoons}} D, \qquad [1]$$

where N and D represent the native and denatured states, respectively, and k_f and k_u are the first-order rate constants for folding and unfolding, respectively. When a protein folds in a two-state fashion, any NMR resonance can be used to determine k_f and k_u. In this study we use the aromatic region of the ^1H NMR spectrum because it shows good spectral dispersion and can be assigned in both the native and denatured states (28), as shown in Fig. 2. The aromatic spectrum of λ_{6-85} at various urea concentrations is shown in Fig. 3. At intermediate

The publication costs of this article were defrayed in part by page charge payment. This article must therefore be hereby marked "*advertisement*" in accordance with 18 U.S.C. §1734 solely to indicate this fact.

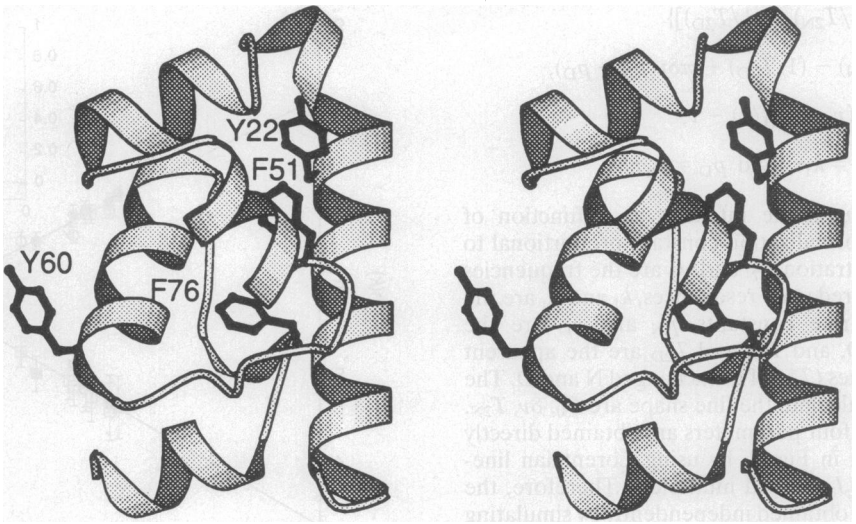

FIG. 1. Stereoview of λ_{6-85} coordinates from the protein–DNA cocrystal structure of Beamer and Pabo (27). Side chains of Tyr-22, Phe-51, Tyr-60, and Phe-76 are indicated. Figure was made with MOLSCRIPT (29).

urea concentrations, each molecule samples both states several times during the acquisition of the NMR spectrum. This exchange process leads to a shift in peak position and line broadening. As shown in Fig. 3, the aromatic ^{1}H resonances of λ_{6-85} show a variety of line widths, depending upon the difference in native and denatured state chemical shifts. The Phe-51 δH resonance (most downfield) is in slow exchange while the Tyr-60 resonances (sharp central peaks) are in fast exchange at all urea concentrations. We chose to use the resonances for Tyr-22 δH and Tyr-22 εH for our kinetic measurements because they display measurable line broadening and can be resolved at most urea concentrations. The Phe-51 εH resonance (Fig. 2, peak i) is substantially broadened by exchange and causes an up-field shoulder on the peak of Tyr-22 εH at urea concentrations <2 M. This shoulder was accounted for in the line-shape analysis.

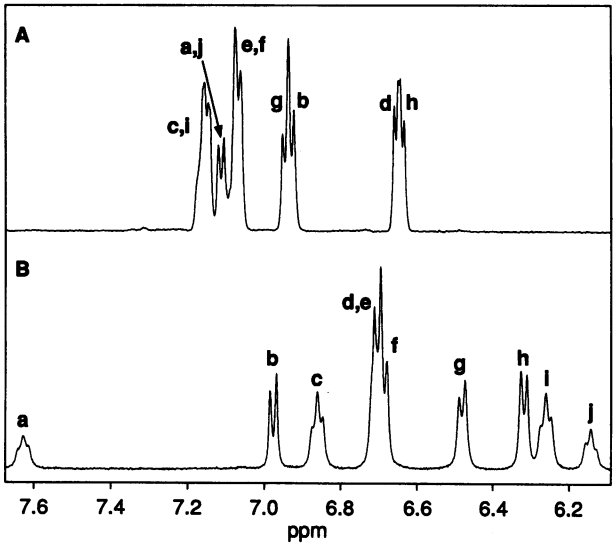

FIG. 2. Aromatic ^{1}H NMR spectra of the λ_{6-85} denatured state in 6.6 M urea (*A*) and the native state in 0 M urea (*B*). NMR samples consisted of 500 μM λ_{6-85} in ≈99% ^2H_2O, 10 mM $C^2H_3COO^2H$, 100 mM NaCl, 3-(trimethylsilyl)propionic acid (17 μg/ml), 1 mM NaN_3, pH 5.6, at 37°C. The chemical shifts of aromatic side-chain protons in the native state are as follows: Tyr-22 δH (g, 6.47), Tyr-22 εH (h, 6.31), Phe-51 δH (f, 6.68), Phe-51 εH (i, 6.25), Phe-51 ζH (j, 6.14), Tyr-60 δH (b, 6.97), Tyr-60 εH (d, 6.70), Phe-76 δH (e, 6.70), Phe-76 εH (c, 6.85), and Phe-76 ζH (a, 7.63).

The spectrum of a protein resonance in two-state exchange between native (N) and denatured (D) states is given by the following equation for the intensity as a function of frequency (13):

$$I(\nu) = -C_0 \frac{\left\{P\left[1 + \tau\left(\frac{p_D}{T_{2N}} + \frac{p_N}{T_{2D}}\right)\right] + QR\right\}}{P^2 + R^2}, \qquad [2]$$

where

$$P = \tau[(1/T_{2N}T_{2D}) - 4\pi^2\Delta\nu^2 + \pi^2(\delta\nu)^2] + (p_N/T_{2N}) + (p_D/T_{2D}),$$

$$Q = \tau[2\pi\Delta\nu - \pi\delta\nu(p_N - p_D)],$$

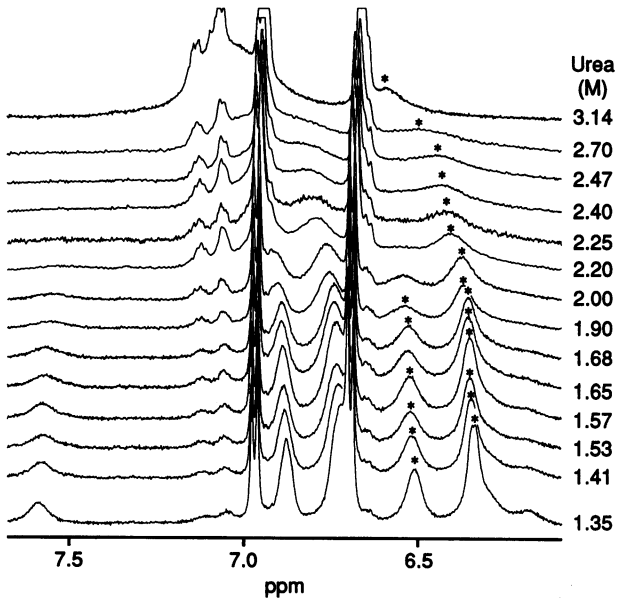

FIG. 3. Aromatic ^{1}H NMR spectra used for line-shape analysis. NMR samples consisted of 500 μM λ_{6-85} in ≈99% ^2H_2O/10 mM $C^2H_3COO^2H$/100 mM NaCl/3-(trimethylsilyl)propionic acid (17 μg/ml)/1 mM NaN_3, pH 5.6, at 37°C. The Tyr-22 resonances used for kinetic analysis are indicated with *.

$$R = 2\pi\Delta\nu\{1 + \tau[(1/T_{2N}) + (1/T_{2D})]\} + \pi\delta\nu\tau[(1/T_{2N}) - (1/T_{2D}) + \pi\delta\nu(p_N - p_D),$$

$$\delta\nu = \nu_N - \nu_D, \Delta\nu = (\nu_N + \nu_D/2) - \nu,$$

$$\tau = 1/(k_u + k_f), p_N = k_f\tau, \text{ and } p_D = k_u\tau.$$

In these equations, $I(\nu)$ is the intensity as a function of frequency (ν), C_0 is a normalization constant proportional to the total protein concentration, ν_N and ν_D are the frequencies of the native and denatured state resonances, k_f and k_u are the folding and unfolding rate constants, p_N and p_D are the populations of N and D, and T_{2N} and T_{2D} are the apparent transverse relaxation times (T_2^*) of unexchanged N and D. The parameters needed to calculate the line shape are C_0, $\delta\nu$, T_{2N}, T_{2D}, k_f, and k_u. The first four parameters are obtained directly from the spectra shown in Fig. 2, by using Lorentzian line-shape simulation of the *J*-coupled multiplets. Therefore, the values of k_f and k_u can be obtained independently by simulating the position and shape of a given resonance. An example of this analysis for Tyr-22 δH at 1.41 M urea is demonstrated in Fig. 4. As demonstrated in Fig. 4*B*, k_f and k_u are sufficiently independent to allow the determination of both parameters with good precision.

This procedure was applied to the resonance for Tyr-22 εH in the ^{1}H spectra of λ_{6-85} obtained at concentrations between 1.35 and 3.14 M urea at 37°C, and the resulting rate constants are depicted in Fig. 5. The uncertainties in k_f and k_u were estimated from a comparison of the residuals at different k_f and k_u combinations as demonstrated in Fig. 4. At <1.35 M urea, the low population of denatured protein precluded accurate fits; at >3.14 M, the resolution of the Tyr-22 peaks from other resonances was too low. However, the range of usable urea concentrations is similar to that of stopped-flow denaturant dilution studies. As a replicate measurement, the position and shape of the resonance for Tyr-22 δH at 1.41 to 1.90 M urea were also simulated. The rate constants measured from this peak are identical to those of Tyr-22 εH (see Fig. 5). Also shown in Fig. 5 is a comparison of the fraction denatured vs. urea curve obtained from equilibrium CD studies (28) and the fraction denatured calculated from the observed values of k_f and k_u. The agreement is striking and provides further evidence that the folding reaction is purely two-state.

The linear relationship between the logarithm of the folding or unfolding rate and urea concentration shown in Fig. 5 has also been demonstrated for many other proteins. This linear relationship allows the estimation of the folding and unfolding rates in the absence of urea by extrapolation. Previous studies on barnase (31) and ubiquitin (3) have revealed a downward curvature in the plot of $\ln(k_f)$ vs. urea. If this curvature exists for λ_{6-85} at urea concentrations <1.35 M, extrapolation to 0 M would overestimate k_f. Because the ^{1}H NMR spectrum of λ_{6-85} is insensitive to urea at low concentrations, it is unlikely that this is the case. However, the value of k_f at 1.35 M urea (1200 s^{-1}) is the lower limit for k_f at 0 M urea and is still an order of magnitude faster than any previously measured protein folding rate.

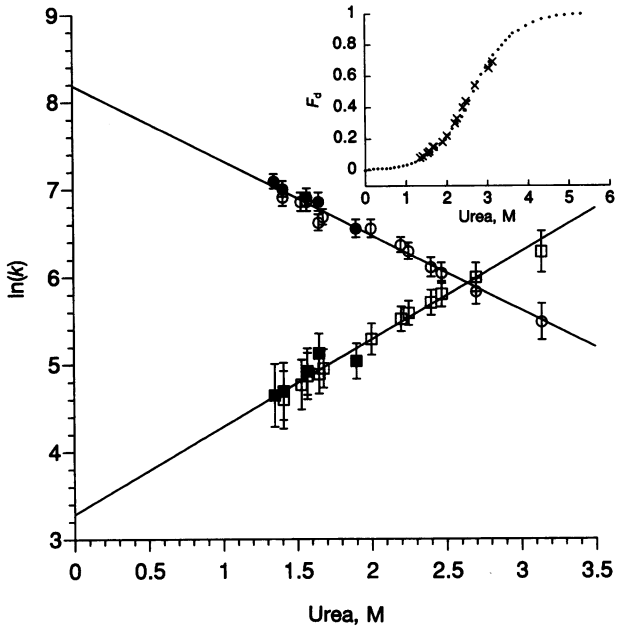

FIG. 5. Natural logarithm of the λ_{6-85} folding (circles) and unfolding (squares) rate constants vs. urea concentration at 37°C. Open symbols are points determined from the Tyr-22 εH resonance; solid symbols are from Tyr-22 δH. The lines indicate weighted best fits of the data (R^2 = 0.97 for both). A folding rate constant 3600 ± 400 s^{-1} and unfolding rate constant of 27 ± 6 s^{-1} in the absence of urea are obtained from the 0 M intercepts of the linear fits. (*Inset*) Comparison between fraction denatured (F_d) as calculated from the equation $F_d = k_u/(k_f + k_u)$ and the curve obtained from CD (see ref. 28).

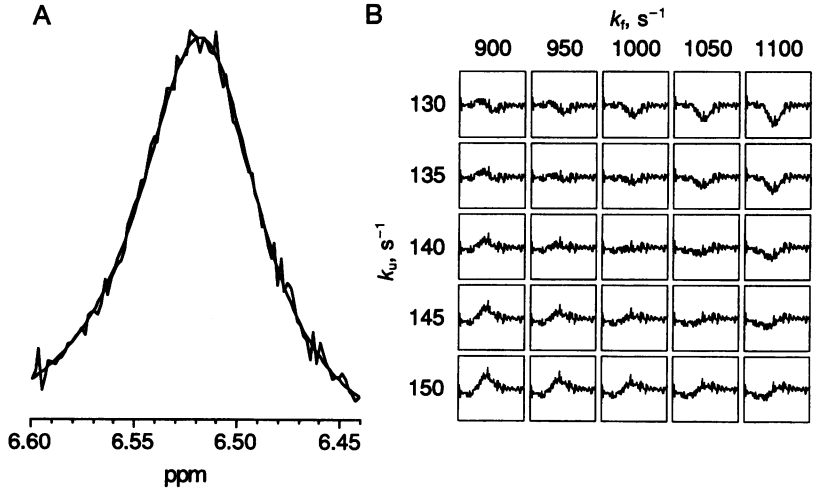

FIG. 4. Line-shape simulation for Tyr-22 δH at 1.41 M urea. (*A*) The observed resonance for Tyr-22 δH (points) and the simulated peak using a folding/unfolding rate of 1000/136 s^{-1}. (*B*) The residuals of the fitting analysis obtained by subtracting the simulated spectrum from the baseline-corrected observed spectrum, shown as a function of the two fitted parameters k_f and k_u near the optimum values. While some covariance between k_f and k_u is observed, only a limited range of k_f and k_u gives good fits.

The extrapolated rate constants are 3600 ± 400 s^{-1} for folding and 27 ± 6 s^{-1} for unfolding. This folding rate constant exceeds the rate constant for the IgG binding domain of streptococcal protein B2 and chymotrypsin inhibitor 2 at 37°C by factors of 45 and 33, respectively (32, 33). λ_{6-85} folds 54 times faster than cytochrome *c* at pH 5 and 10°C (34), 56 times faster than 4 μM Arc repressor at 31°C (23), and 14 times faster than ubiquitin at 8°C (3). Based on the observed folding rates, any partially folded intermediates formed during the folding or unfolding of λ_{6-85} would have lifetimes shorter than 330 μs, well under the dead time of all current stopped-flow instruments. The rapid folding rate we observe presents an experimental challenge for characterizing the folding pathway of λ_{6-85}, but it establishes that all the fundamental steps required for complete folding of a stable globular protein can occur at rates much faster than previously measured.

The method used in this study is not time-resolved so it cannot detect short-lived intermediates, but it can be used to study the transition state for folding. At 37°C in the absence of urea, the activation energies for forming the transition state from the native and denatured states are 16.1 ± 0.1 and 13.1 ± 0.1 kcal/mol (1 cal = 4.184 J), respectively (35). Further studies of the temperature dependence of these activation energies should provide insights into the thermodynamic properties of the transition state. The linearity of the plots in Fig. 5 (R^2 = 0.97) indicates that from 1.35 to 3.14 M urea (9–69% denatured), the rate-determining step for folding does not change. Weighted least-squares fits of $\ln(k_f)$ and $\ln(k_u)$ vs. urea concentration data shown in Fig. 5 give slopes of −0.86 ± 0.06 M^{-1} and 1.0 ± 0.1 M^{-1}, respectively. These slopes can be related to m_f and m_u, the urea dependence of the activation energies, by multiplying by *RT* (0.614 kcal/mol). For a two-state folding reaction, the quantity ($m_u - m_f$) should be equivalent to the slope of the free energy of denaturation vs. urea curve obtained from equilibrium studies (35). For λ_{6-85}, $m_u - m_f$ obtained from kinetic studies is 1.15 ± 0.1 kcal per mol per M, in good agreement with a value of 1.23 ± 0.1 kcal per mol per M determined in previous thermodynamic studies (28). The fractional exposure of the transition state to solvent, relative to that exposed upon complete denaturation, can be estimated from $m_u/(m_u - m_f)$ or $\alpha^{\ddagger}$ (35). This quantity is 0.54 ± 0.06, indicating that the amount of area exposed in forming the transition state is more than half of that exposed upon denaturation. This is considerably more than observed for other proteins (0.25–0.4) (23, 33, 35), suggesting that the λ_{6-85} transition state is more solvent-exposed than those of more slowly folding proteins.

Why does λ_{6-85} fold so fast? Its relatively small size (80 residues) must be part of the explanation, since larger proteins are inevitably more complex and more likely to require slow conformational changes. However, several proteins of similar size or smaller have considerably slower folding rates, so small size alone is insufficient to produce rapid folding. The truncations used to produce a monomeric version of λ repressor are unlikely to cause fast folding because the residues removed at the N terminus are disordered in solution. Furthermore, the ^{1}H NMR spectrum of a disulfide-linked version of λ_{1-102} dimer appears to show similar exchange broadening (36), indicating that it folds at a similar rate.

The secondary structure of the native state may play a key role in determining the overall folding rate. Among proteins of similar size or smaller whose folding rates have been measured, λ_{6-85} is the only one without β structure. The inherently short-range interactions (3 or 4 residues) that stabilize helices may form more rapidly than the long-range interactions found in most β structure. Interestingly, *lac* repressor headpiece, a 51-residue all-helical protein, shows NMR spectra indicative of folding at least as fast as λ_{6-85} (25). It has also been proposed that the α-helix is the most formed of all secondary structure in the transition state of chymotrypsin inhibitor 2 (37). As an extension of submicrosecond estimates for helix formation in homopolymers, these data suggest that α-helix is an inherently fast-folding secondary structure in globular proteins as well.

Whatever the reason for the fast folding of λ_{6-85}, it may play an important role in the biological function of the protein. It is important to note that previous denaturation studies of intact λ repressor indicate that the N- and C-terminal domains fold independently with melting temperatures of ≈50 and ≈80°C, respectively (38). Thus, the unfolding of λ_{6-85} should be a good model for the most likely first step in the unfolding of the full-length protein. At 37°C, in the absence of denaturant, the half-life for unfolding of the native state of λ_{6-85} is only 41 ms, calculated from the extrapolated value of k_u. The folding half-life for the denatured state under these conditions is 230 μs. Thus, under physiological conditions, λ_{6-85} (and by inference the N-terminal domain of the free protein) is undergoing constant unfolding/refolding. Unfolding may represent a crucial rate-limiting step in the proteolysis of more slowly folding proteins. Given the role that repressor concentration plays in the life cycle of phage λ, rapid proteolytic degradation of the frequently unfolded free protein may play a crucial role in its biological function. Further studies are necessary to determine whether unfolding rate decreases when the protein is bound as a dimer to its cognate DNA. Rapid folding may also be a consequence of an evolved flexibility required for efficient DNA binding. The fast folding observed for Arc repressor monomer (23) and *lac* repressor (25) suggests that this may be an important property of similar repressor proteins.

Despite its fast folding, λ_{6-85} must undergo the same fundamental steps in folding as all other proteins. These steps include collapse of the polypeptide chain, initiation of secondary structure, desolvation of buried groups, and packing of side chains. Sosnick *et al.* (34) have concluded that the formation of a collapsed molten-globule-like state is the intrinsic rate-limiting step in the folding of cytochrome *c* at low pH and that subsequent steps such as solvent extrusion and side-chain packing are not inherently slow. In cytochrome *c*, the collapse takes ≈15 ms (34), but in λ_{6-85}, it must occur within ≈0.3 ms. Given the nonspecific nature of chain collapse, this discrepancy seems quite large and suggests that other slow steps may slow the folding of cytochrome *c*. An important distinction between the method described here and time-resolved methods is that our measurements are made under equilibrium conditions. For this reason, it is possible that line broadening is caused by exchange between the native state and an incompletely denatured (i.e., precollapsed) state in slow exchange with the completely denatured state. The evidence against this possibility comes from the agreement between the kinetic and equilibrium data shown in Fig. 5 and detailed denaturation studies that show identical denaturation curves for λ_{6-85} as detected by CD and the ^{1}H chemical shifts of the four aromatic residues (28). For these curves to superimpose, the NMR and CD spectra of the partially denatured state would have to be identical to those of the denatured state. Given the sensitivity of NMR chemical shifts to local environment, this situation seems highly unlikely. Further studies are necessary to identify the fundamental rate-limiting step in folding but our results clearly demonstrate that it can occur on the submillisecond time scale for an 80-residue helical protein.

Our results, combined with those reported recently for several other fast-folding systems (32, 34, 37, 39), lead to a consistent picture of protein folding transition states. It now appears that, even in the absence of obvious kinetic traps, the rate-determining step for folding can occur at various places along the reaction pathway. For barnase, the rate-determining step appears to be the docking of preformed modules of secondary structure (37). For barley chymotrypsin inhibitor 2 (37), the immunoglobulin binding domain of streptococcal protein G (32, 39), and cytochrome *c* at low pH (34), the rate-determining step appears to be the rearrangement of col-

lapsed structure into regular secondary structure. The relatively large value of $m_u/(m_u - m_f)$ for λ_{6-85} suggests that the rate-determining step occurs earlier in folding, with a less-compact transition state. This preliminary evidence suggests that there may be a correlation between the rate of folding (magnitude of activation energy) and the position of the rate-limiting step on the reaction pathway. Early rate-limiting steps appear to have lower activation barriers, while late rate-limiting steps involve high-energy transition states with a large amount of native-like structure. In addition to having lower activation energies, it has been proposed that early transition states may involve a larger number of chain conformations that would also accelerate folding (40).

The ability to measure protein folding and unfolding rates on the submillisecond time scale opens a large number of experimental opportunities to characterize the mechanisms of rapid protein folding reactions. Many of the tools used to characterize protein folding transition states by stopped-flow methods are applicable to the dynamic NMR approach. These include site-directed mutagenesis (41), Arrhenius analysis (35), and solvent perturbation studies. For these studies, small rapidly folding proteins such as λ_{6-85} are good model systems for the early events in the folding of all proteins.

We thank Wendell Lim for sharing his λ_{6-85} construct and Michael Strain for the line shape simulation program. We are grateful to Marcos Milla, Tobin Sosnick, Walter Englander, and Heinrich Roder for useful discussions and Peggy Daugherty, Carol Fierke, and Peter Kim for comments on the manuscript. This work was supported by National Institutes of Health Grant GM45322 and by American Cancer Society Junior Faculty Research Award JFRA-398.

1. Baldwin, R. L. (1989) *Trends Biochem. Sci.* **14,** 291–294.
2. Wright, P. E., Dyson, H. J. & Lerner, R. A. (1988) *Biochemistry* **27,** 7167–7175.
3. Khorasanizadeh, S., Peters, I. D., Butt, T. R. & Roder, H. (1993) *Biochemistry* **32,** 7054–7063.
4. Bycroft, M., Matouschek, A., Kellis, J. T., Jr., Serrano, L. & Fersht, A. R. (1990) *Nature (London)* **346,** 488–490.
5. Briggs, M. S. & Roder, H. (1992) *Proc. Natl. Acad. Sci. USA* **89,** 2017–2021.
6. Lu, J. & Dahlquist, F. W. (1992) *Biochemistry* **31,** 4749–4756.
7. Roder, H., Elöve, G. A. & Englander, S. W. (1988) *Nature (London)* **335,** 700–704.
8. Radford, S. E., Dobson, C. M. & Evans, P. A. (1992) *Nature (London)* **358,** 302–307.
9. Udgaonkar, J. B. & Baldwin, R. L. (1990) *Proc. Natl. Acad. Sci. USA* **87,** 8197–8201.
10. Lang, J., Tondre, C. & Zana, R. (1971) *J. Phys. Chem.* **75,** 374–379.
11. Hammes, G. G. & Roberts, P. B. (1969) *J. Am. Chem. Soc.* **91,** 1812–1816.
12. Schwarz, G. & Seelig, J. (1968) *Biopolymers* **6,** 1263–1277.
13. Sandström, J. (1982) *Dynamic NMR Spectroscopy* (Academic, New York).
14. Brünger, A. T., Huber, R. & Karplus, M. (1987) *Biochemistry* **26,** 5153–5162.
15. Levy, R. M. & Karplus, M. (1981) *J. Am. Chem. Soc.* **103,** 994–996.
16. Kay, L. E., Torchia, D. A. & Bax, A. (1989) *Biochemistry* **28,** 8972–8979.
17. Olejniczak, E. T., Dobson, C. M., Karplus, M. & Levy, R. M. (1984) *J. Am. Chem. Soc.* **106,** 1923–1930.
18. Ropson, I. J. & Frieden, C. (1992) *Proc. Natl. Acad. Sci. USA* **89,** 7222–7226.
19. Benz, F. W. & Roberts, G. C. K. (1975) *J. Mol. Biol.* **91,** 345–365.
20. Bradbury, J. H. & King, N. L. R. (1969) *Nature (London)* **223,** 1154–1156.
21. McDonald, C. C., Phillips, W. D. & Glickson, J. D. (1971) *J. Am. Chem. Soc.* **93,** 235–246.
22. Westmoreland, D. G. & Matthews, C. R. (1973) *Proc. Natl. Acad. Sci. USA* **70,** 914–918.
23. Milla, M. E. & Sauer, R. T. (1994) *Biochemistry* **33,** 1125–1133.
24. Oas, T. G. & Kim, P. S. (1988) *Nature (London)* **336,** 42–48.
25. Wemmer, D., Ribeiro, A. A., Bray, R. P., Wade-Jardetzky, N. G. & Jardetzky, O. (1981) *Biochemistry* **20,** 829–833.
26. Sauer, R. T., Jordan, S. R. & Pabo, C. O. (1990) *Adv. Protein Chem.* **40,** 1–61.
27. Beamer, L. J. & Pabo, C. O. (1992) *J. Mol. Biol.* **227,** 177–196.
28. Huang, G. S. & Oas, T. G. (1995) *Biochemistry* **34,** 3384–3892.
29. Kraulis, P. K. (1991) *J. Appl. Crystallogr.* **24,** 946–950.
30. Pace, C. N. (1986) *Methods Enzymol.* **131,** 266–280.
31. Matouschek, A., Matthews, J. M., Johnson, C. M. & Fersht, A. R. (1994) *Protein Eng.* **7,** 1089–1095.
32. Alexander, P., Orban, J. & Bryan, P. (1992) *Biochemistry* **31,** 7243–7248.
33. Jackson, S. E. & Fersht, A. R. (1991) *Biochemistry* **30,** 10436–10443.
34. Sosnick, T. R., Mayne, L., Hiller, R. & Englander, S. W. (1994) *Struct. Biol.* **1,** 149–156.
35. Chen, B.-L., Baase, W. A., Nicholson, H. & Schellman, J. A. (1992) *Biochemistry* **31,** 1464–1476.
36. Weiss, M. A., Pabo, C. O., Karplus, M. & Sauer, R. T. (1987) *Biochemistry* **26,** 897–904.
37. Otzen, D. E., Itzhaki, L. S., Elmasry, N. F., Jackson, S. E. & Fersht, A. R. (1994) *Proc. Natl. Acad. Sci. USA* **91,** 10422–10425.
38. Pabo, C. O., Sauer, R. T., Sturtevant, J. & Ptashne, M. (1979) *Proc. Natl. Acad. Sci. USA* **76,** 1608–1612.
39. Kuszewski, J., Clore, G. M. & Gronenborn, A. M. (1994) *Protein Sci.* **3,** 1945–1952.
40. Abkevich, V. I., Gutin, A. M. & Shakhnovich, E. I. (1994) *Biochemistry* **33,** 10026–10036.
41. Matouschek, A., Kellis, J. J., Serrano, L. & Fersht, A. R. (1989) *Nature (London)* **340,** 122–126.